Brazilian Journal
of Chemical
Engineering

ISSN 0104-6632
Printed in Brazil
www.abeq.org.br/bjche

Vol. 32, No. 04, pp. 875 - 893, October - December, 2015
dx.doi.org/10.1590/0104-6632.20150324s00003584

SELECTIVE CATALYTIC REDUCTION (SCR) OF NO BY AMMONIA OVER V_2O_5/TiO_2 CATALYST IN A CATALYTIC FILTER MEDIUM AND HONEYCOMB REACTOR: A KINETIC MODELING STUDY

M. Nahavandi

Department of Chemical and Materials Engineering, University of Idaho, Moscow, ID 83844, USA.
Phone: (+1) 208 596 7659
E-mail: Milad@uidaho.edu

(Submitted: June 19, 2014 ; Revised: January 11, 2015 ; Accepted: February 2, 2015)

Abstract - The present study addresses a numerical modeling and simulation based on the available knowledge of SCR kinetics for prediction of NO conversion over a V_2O_5/TiO_2 catalyst through a catalytic filter medium and honeycomb reactor. After introducing the NH_3-SCR system with specific operational criteria, a reactor model was developed to evaluate the effect of various operating parameters such as flue gas temperature, velocity, NH_3/NO molar ratio, etc., on the SCR process. Computational investigations were performed based on the proposed model and optimum operational conditions were identified. Simulation results indicate that SCR performance is substantially under the effects of reactant concentration and operating temperature, so that the concentration of unreacted ammonia emitted from reactor discharge (ammonia slip) increases significantly at NH_3/NO ratios of more than 1.14 and operating temperatures less than 360 ºC and 300 ºC, respectively, in the catalytic filter medium and honeycomb reactor. The results also show that there are three sections in NO conversion variation versus changing temperature and the required conversion with a maximum of almost 87% and low level of ammonia slip can be achieved at the NH_3/NO ratio of 1 and temperature range of 240–360 ºC in both reactors.
Keywords: Exhaust fume cleaning; Selective Catalytic Reduction (SCR); NH_3-SCR System; Ammonia slip; NO conversion; Catalytic filter medium; Honeycomb reactor.

INTRODUCTION

The concentration of anthropogenic and toxic pollutants in the atmosphere has increased rapidly throughout the last decades, which is basically due to the combustion of fossil fuels and biomass. In recent years, the problem of air pollution caused by toxic gases such as NO_x and SO_x, has become ecologically serious. Nitrogen oxides (NO_x) are a group of air pollutants, including nitrogen oxide, nitrogen dioxide and nitrous oxide, considered as very dangerous, since they contribute to the greenhouse effect and participate in photochemical reactions that lead to acid rain, tropospheric ozone and respiratory problems in humans (Vega *et al*., 2011). So, the reduction of NO_x from stationary and mobile sources has become an important concern of industrialized countries, due to an increased attention to environmental pollution and to the demand for sustainable energy development. Hence, the elimination of gaseous pollutants and particles from high temperature gases is often required in waste incineration and thermal power plants. There are two sources of NO_x. One of them occurs in nature (nitrogen fixation by lightning, volcanic activity, oxidation of ammonia in the troposphere, inflow of NO from the stratosphere, ammo-

*To whom correspondence should be addressed

nia oxidation from the decompositions of proteins). The other is the combustion of fossil fuels (especially in vehicles) that is the main cause of emissions (Nova *et al*., 2006).

Several techniques seem to be feasible for NO_x abatement, such as cooled EGR, common rail fuel injection, LNT, LNC, and SCR $DeNO_x$ systems (Ciardelli *et al*., 2007). Three major ones are lean NO_x traps (LNT), ammonia- or urea- Selective Catalytic Reduction (NH_3-SCR) and Hydrocarbons Selective Catalytic Reduction (HC-SCR). The control of NO_x emissions from stationary sources includes techniques of modification of the combustion stage (primary measures) and treatment of the effluent gases (secondary measures). The primary measures, which are extensively applied, guarantee NO_x reduction levels of the order of 50 to 60%: this may not fit the most stringent legislations of many countries. Among the secondary measures, a well-established technology is represented by the ammonia selective catalytic reduction process (NH_3-SCR). This method, which was established in the 1970s, has been used mainly for stationary sources and still is the major strategy for the reduction of NO, industrially, due to its high efficiency and the ability of ammonia to react selectively with NO_x to form nitrogen (N_2) and water (H_2O), together with the resistance to poisoning and aging of the applied catalysts (Vega *et al*., 2011).

Also, in term of the SCR catalyst, the application of a V_2O_5/TiO_2 catalyst in the SCR process is very effective. This catalyst could be widely used in Euro IV/V engines without filters and, due to the resistance of V_2O_5-based formulations to sulfur poisoning, it can also be the preferred SCR catalyst choice for various applications (Yun and Kim, 2013; Kobayashi *et al*., 2004).

So far, a number of investigations have been reported on the selective catalytic reduction of NO by NH_3 as a reductant (reducing agent) over Vanadia-based catalysts to improve the reduction performance. Winkler *et al*. (2003) developed a one-dimensional numerical model for chemical reactions to describe the $DeNO_x$ behavior of a current commercial SCR catalyst by considering both standard and fast SCR reactions with the oxidation of NH_3. They also carried out a parametric study by changing the concentrations of various components such as NO, NH_3 etc. to find the effects on SCR performance using FTIR spectrometry and computational investigation. The heterogeneous chemical reactions taking place on the catalytic surface are also taken into account based on the Langmuir-Hinshelwood (LH) mechanism, while the NH_3 storage phenomena are adopted through the Dubinin-Radushkevich adsorption isotherm (Tsinoglou and Koltsakis, 2007). To evaluate the $DeNO_x$ performance, Gieshoff *et al*. (2000) carried out studies and changed parameters such as the NH_3/NO_x and the NO_2/NO_x ratios over a V_2O_5 catalyst. Also, in an effort to improve the NO_x conversion efficiency, several investigations have been performed using parameters such as space velocity, the temperature of the SCR catalyst, and the volume of oxidation catalyst, at different raw NO_x concentrations (Nam, 2007). Lietti *et al*. (1997) performed numerical investigations to determine the $DeNO_x$ behavior over a V_2O_5 SCR catalyst by changing various parameters such as NH_3 concentration, the temperature of the SCR catalyst, and NH_3/NO ratio. Furthermore, Nova *et al*. (2006; 2009) conducted a kinetic modeling of SCR reactions over a Vanadia-based catalysts for heavy duty diesel applications.

Even so, there are few investigations concerning NH_3-SCR of NO over Vanadia-based catalysts in a catalytic filter and honeycomb reactor. These multifunctional reactors for the simultaneous filtration and selective catalytic reduction (SCR) of NO_x in high-temperature gas cleaning are of industrial interest since they allow substitution of two or more process units with a single reactor, where all the operations of interest are executed simultaneously. They have been suggested to save energy, space and cost and are capable of carrying out, besides the chemical reactions, other functions, such as separation or heat exchange. Schaub *et al*. (2003) studied NH_3-SCR of nitric oxide (NO) over V_2O_5/TiO_2 in a catalytic filter using numerical kinetic modeling. They found that NO conversion of 60-80% is possible on the time scales of gas flow through the catalytic filter medium for temperatures around 250-350 °C. They also developed their model to indirectly reach some sort of validation for a SCR honeycomb reactor. Zurcher *et al*. (2008) experimentally investigated NH_3-SCR of NO over two catalyst configurations namely ceramic candle and ceramic sponges, impregnated with $V_2O_5/TiO_2/WO_3$-based catalysts, in a fixed-bed reactor and individually. Results showed that the highest conversion values at 300 °C for both configurations in a fixed-bed reactor were generally lower in multifunctional reactors. Hubner *et al*. (1996) carried out an experimental investigation on NH_3-SCR of NO with a filter medium made from ceramic fibers on laboratory and bench scales, using model flue gases and a real flue gas from fuel oil combustion; filter candles were used and impregnated with various SCR catalysts (vanadium-oxide and others). Also, Roduit *et al*. (1998) developed a 3D modeling for selective catalytic reduction of NO_x by NH_3 over Vanadia honey-

comb catalysts. In the most recent study, Nahavandi (2014) performed a numerical investigation of the enhancing effect of the electrohydrodynamics (EHD) technique on NH_3-SCR of NO over V_2O_5/TiO_2 in a hollow cylindrical catalyst. Based on the obtained results, the maximum enhancement of almost 4.2-fold could be achieved for NO conversion by application of this technique in this type of catalyst.

However, limited experimental and numerical data have been reported in the literature on a catalytic filter medium and honeycomb reactor. In this article, the selective catalytic reduction (SCR) of NO by NH_3 over a V_2O_5/TiO_2 catalyst, together with simultaneous effects of geometrical and operational parameters as well as contour plots of reacting flow in both of these reactors, are thoroughly investigated in a wide range of operating conditions by means of Computational Fluid Dynamics (CFD). The primary objective of this study is to numerically identify the most appropriate operational conditions in which the maximum SCR performance for NO reduction can be achieved, which has not been done so far on these scales and operating ranges in any other publication.

CHEMICAL REACTIONS

The NH_3-SCR reduction of NO over a V_2O_5/TiO_2 catalyst can be described by a reaction network that involves two parallel reactions. The desired reaction is the conversion of NO to N_2 according to Equation (1), while NH_3 oxidation with O_2, based on Equation (2) is an undesired reaction which leads to lower NO conversion and becomes more significant at higher temperatures. The reduction of NO_x is considered to be faster compared to NO, so that NO_x typically consists of up to 95% NO, especially at high temperatures. Therefore, NO_2 is not included in the present study (Schaub *et al*., 2003).

$$4NO + 4NH_3 + O_2 \rightarrow 4N_2 + 6H_2O \quad (1)$$

$$4NH_3 + 3O_2 \rightarrow 2N_2 + 6H_2O \quad (2)$$

NH_3-SCR SYSTEM

The NH_3-SCR System is generally comprised of an aqueous ammonia storage, air supplier, heater, heat exchanger, vaporizer, mixer, injector and SCR reactor. A typical diagram for a NH_3-SCR system is illustrated in Figure 1. As shown, aqueous ammonia is pumped into the vaporizer before being mixed with hot air. Then, gaseous ammonia as a reducing agent (reductant) is injected into flue gas that is preheated in the heat exchanger. After that, the gas mixture flows into the SCR reactor. Then, discharged clean gas flows into the heat exchanger to release its heat to input flue gas. In the SCR process, a gaseous reductant is typically pure anhydrous ammonia, aqueous ammonia or urea. The chemical reactions that occur in NH_3-SCR systems are shown in Equation (1) and (2) where the first one is the desired reaction. The SCR process requires a precise control of the ammonia injection rate. An insufficient injection may result in unacceptably low NO_x conversions. An injection rate that is too high results in release of undesirable ammonia to the atmosphere. These ammonia emissions from SCR systems are known as ammonia slip. The ammonia slip increases at higher NH_3/NO_x ratios. The stoichiometric NH_3/NO_x ratio in the SCR system is about 1. Ratios higher than 1 significantly

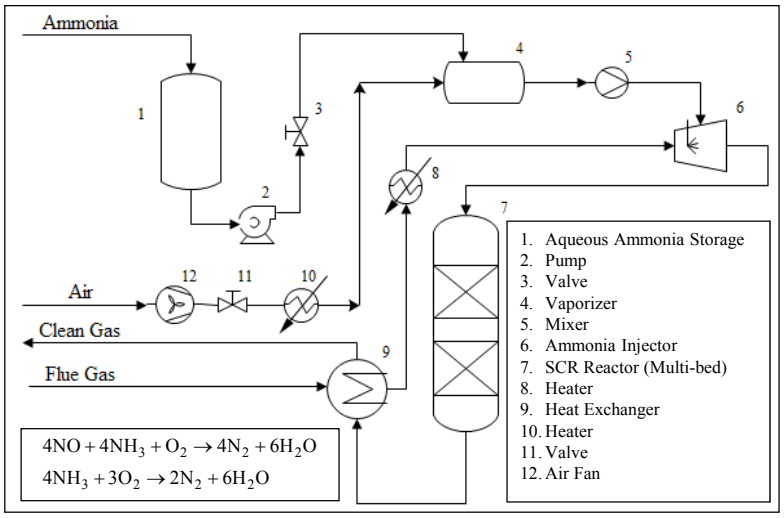

Figure 1: A typical flow diagram of an SCR system.

increase the ammonia slip (Baukal Jr, 2013). In a practical SCR system, ammonia is typically injected to produce a NH_3/NO_x molar ratio of 1.05–1.1 to achieve a NO_x conversion of 80–90% with an ammonia slip of about 10 ppm of unreacted ammonia in gases leaving the reactor. The NO_x removal efficiency depends on the flue gas temperature, the molar ratio of ammonia to NO_x, and the flue gas residence time in the catalyst bed (Neuffer and Laney, 2007). As discussed later, the ammonia slip decreases by increasing temperature, while the NO_x conversion in a SCR catalyst may either increase or decrease with temperature, depending on the particular temperature range and catalyst system. Also, in the following, the effect of NH_3/NO_x ratio on NO conversion is shown in different operating conditions and in the both kinds of SCR reactors.

MODELING AND SIMULATION

Model Definition

The respective models of a honeycomb reactor and an idealized catalytic filter, as commonly used today, are shown respectively in Figure 2 (A) and (B). The geometrical features, together with catalyst properties used in different operating conditions for the simulation of both reactor models, are reported in Table 1.

In these models, the catalytic filter like the honeycomb reactor is assumed to have many narrow quasi-pipe channels in its catalytic porous medium. So, an orthogonal rectangular field as the longitudinal cross-section of one proposed channel along the fluid flow was taken into consideration. Figure 3 (A) shows the proposed channel and its interior catalyst layer, together with the rectangular cross-section. In order to see the entire geometry in one domain, as the length of the channel is much longer than its width, the channel`s length was scaled down 10^3-fold. As can be seen from Figure 3 (B), due to symmetric condition of flow across the channel, the symmetry boundary condition was set to the left boundary. Also, wall and symmetry boundary conditions were set to the right boundary of the catalytic filter and honeycomb reactor, respectively. Two other boundary conditions at the bottom and top of the channel represent the input and output of reacting flow, respectively, with proposed reactant concentrations and gas velocity at the inlet and convective concentrations with no viscous stress at the outlet, under isothermal conditions. The respective boundary conditions are presented in Table 2.

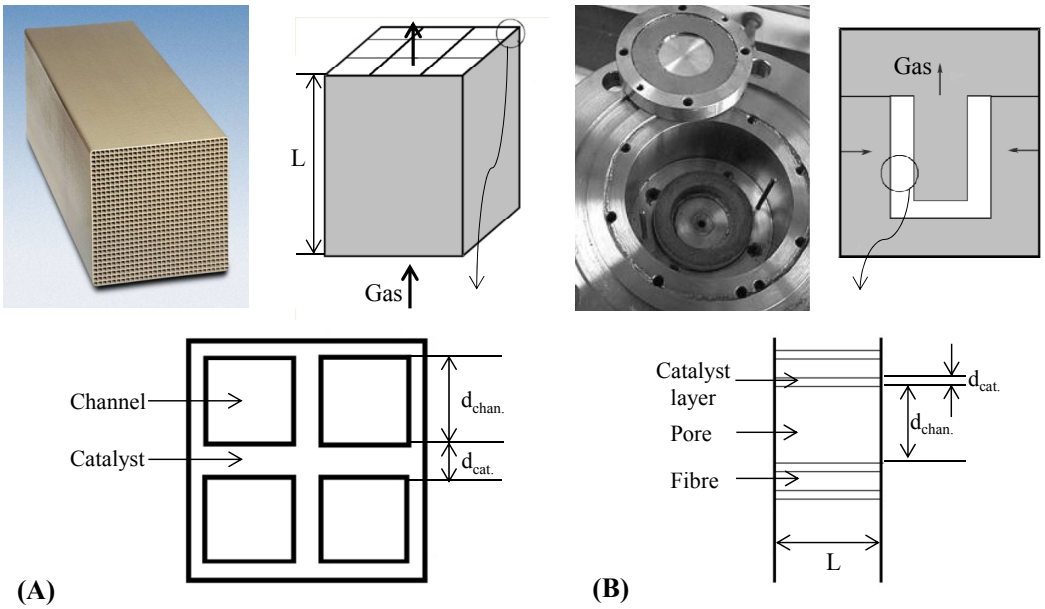

Figure 2: Sketch of a honeycomb reactor (left) and an idealized catalytic filter (right), with geometric definitions used in Table 1.

Table 1: The properties of the catalytic filter and honeycomb reactor for catalyst model simulation.

Operational Parameters		SCR honeycomb	Catalytic filter (rigid or fibre material)
Geometry			
Filter medium thickness (L)	m	0.7- 1.4 - 3	0.009 - 0.02
d_{chan}	mm	3 - 12	0.015
d_{cat}	mm	0.5 - 1.5 (wall thickness)	0.001 (layer thickness)
Catalyst Properties			
Catalyst		V_2O_5/TiO_2 porous homogeneous solid	V_2O_5+ other components impregnated support
V_2O_5 content	wt.%	1 - 3.45	0.5 - 10.4
Porosity (ε_p)	vol.%	64 - 82.5	95
Permeability (k_p)	m^2	10^{-8} [a]	10^{-8} [a]
Operating condition			
Temperature (T)	ºC	200 - 420	160 - 420
GHSV	h^{-1}	5000 - 15000 - 30000	3000 - 5000 - 8000 - 11000
O_2 Inlet concentration (C_{O2})	vol. %	7.6	7.6
NH_3 Inlet concentration (C_{NH3})	ppm	100 - 600	200 - 700
NO Inlet concentration (C_{NO})	ppm	350 - 500	350 - 500

Source: Schaub *et al*. (2003).

[a]Extrapolated for $\varepsilon_p = 82.5$ from the respective results (Seong, 2012).

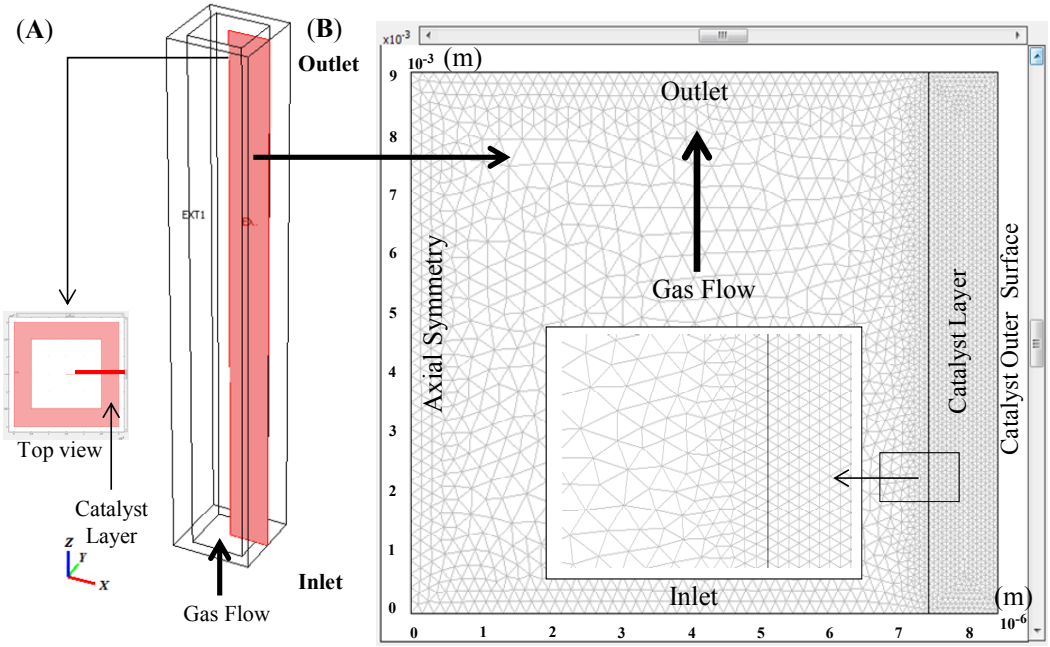

Figure 3: The model geometry consists of gas flow beside the catalyst layer: (A) geometrical shape; (B) grid plot.

Table 2: Boundary conditions.

Variables	Setting				
	inlet[a]	outlet	catalyst outer surface		symmetry
			catalytic filter	honeycomb	
u	$2 \times u_{in} \times (1 - s^2)$	$\eta\left(\nabla u + (\nabla u)^T\right) n = 0$	0	axial sym.	axial sym. x=0
c	c_{j_in}	$n.\left(-D_c \nabla c_j\right) = 0$	$n.\left(-D_c \nabla c_j + c_j u\right) = 0$	axial sym.	axial sym. x=0
T	T_{in}	$n \cdot \left(-k \nabla T\right) = 0$	$n \cdot \left(-k \nabla T\right) = 0$	axial sym.	axial sym. x=0

[a]The value of "s" runs from 0 to 1 along the boundary.

Subdomain Equations

The stationary incompressible Navier–Stokes equation for catalyst-free channels and the Brinkman equation for catalyst porous medium, together with their continuity equations for momentum balance, were used in addition to convection-conduction heat transfer and convection-diffusion mass transfer equations to describe a steady-state laminar flow of reacting gas through the catalytic filter medium and honeycomb reactor, which were solved simultaneously. These equations are illustrated in Equations (3) – (6), respectively.

Navier–Stokes equation (Catalyst pore space)

$$\rho(U\cdot\nabla)U-\nabla\cdot\left[-pI+\eta\left(\nabla U+(\nabla U)^{T}\right)\right]=0$$
$$\Rightarrow\begin{cases}\rho\left(u\dfrac{\partial u}{\partial x}+v\dfrac{\partial u}{\partial z}\right)-\left(\dfrac{\partial}{\partial x}\left(2\eta\dfrac{\partial u}{\partial x}-P\right)+\dfrac{\partial}{\partial z}\left(\eta\left(\dfrac{\partial u}{\partial z}+\dfrac{\partial v}{\partial x}\right)\right)\right)=0\\ \rho\left(u\dfrac{\partial v}{\partial x}+v\dfrac{\partial v}{\partial z}\right)-\left(\dfrac{\partial}{\partial x}\left(\eta\left(\dfrac{\partial v}{\partial x}+\dfrac{\partial u}{\partial z}\right)\right)+\dfrac{\partial}{\partial z}\left(2\eta\dfrac{\partial v}{\partial z}-P\right)\right)=0\end{cases} \tag{3}$$

Continuity equation

$$\frac{\partial u}{\partial x}+\frac{\partial v}{\partial z}=0 \tag{3a}$$

Brinkman equation (Catalyst layer)

$$\left(\frac{\eta}{k_p}\right)U-\nabla\cdot\left[-pI+\left(\frac{1}{\varepsilon_p}\right)\left\{\eta\left(\nabla U+(\nabla U)^{T}\right)-\left(\frac{2\eta}{3}\right)(\nabla\cdot U)I\right\}\right]=0$$
$$\Rightarrow\begin{cases}\left(\dfrac{\eta}{k_p}\right)u-\left(\dfrac{\partial}{\partial x}\left(\left(\dfrac{1}{\varepsilon_p}\right)\left\{2\eta\dfrac{\partial u}{\partial x}-\left(\dfrac{2\eta}{3}\right)\left(\dfrac{\partial u}{\partial x}+\dfrac{\partial v}{\partial z}\right)\right\}-P\right)+\dfrac{\partial}{\partial z}\left(\left(\dfrac{1}{\varepsilon_p}\right)\left\{\eta\left(\dfrac{\partial u}{\partial z}+\dfrac{\partial v}{\partial x}\right)\right\}\right)\right)=0\\ \left(\dfrac{\eta}{k_p}\right)v-\left(\dfrac{\partial}{\partial x}\left(\left(\dfrac{1}{\varepsilon_p}\right)\left\{\eta\left(\dfrac{\partial v}{\partial x}+\dfrac{\partial u}{\partial z}\right)\right\}\right)+\dfrac{\partial}{\partial z}\left(\left(\dfrac{1}{\varepsilon_p}\right)\left\{2\eta\dfrac{\partial v}{\partial z}-\left(\dfrac{2\eta}{3}\right)\left(\dfrac{\partial u}{\partial x}+\dfrac{\partial v}{\partial z}\right)\right\}-P\right)\right)=0\end{cases} \tag{4}$$

Energy balance

$$\rho C_p U\cdot\nabla T=\nabla\cdot\left(k\nabla T\right)$$
$$\Rightarrow\rho C_p\left(u\frac{\partial T}{\partial x}+v\frac{\partial T}{\partial y}\right)-\left(\frac{\partial}{\partial x}\left(k\frac{\partial T}{\partial x}\right)+\frac{\partial}{\partial y}\left(k\frac{\partial T}{\partial y}\right)\right)=0 \tag{5}$$

Component mass balance

$$U\cdot\nabla C_i=\nabla\cdot\left(D_c\nabla C_i\right)+R_i$$
$$\Rightarrow\begin{cases}\left(u\dfrac{\partial C_{NO}}{\partial x}+v\dfrac{\partial C_{NO}}{\partial y}\right)-\left(\dfrac{\partial}{\partial x}\left(D_c\dfrac{\partial C_{NO}}{\partial x}\right)+\dfrac{\partial}{\partial y}\left(D_c\dfrac{\partial C_{NO}}{\partial y}\right)\right)=-4R_1\\ \left(u\dfrac{\partial C_{NH_3}}{\partial x}+v\dfrac{\partial C_{NH_3}}{\partial y}\right)-\left(\dfrac{\partial}{\partial x}\left(D_c\dfrac{\partial C_{NH_3}}{\partial x}\right)+\dfrac{\partial}{\partial y}\left(D_c\dfrac{\partial C_{NH_3}}{\partial y}\right)\right)=-4\left(R_1+R_2\right)\\ \left(u\dfrac{\partial C_{O_2}}{\partial x}+v\dfrac{\partial C_{O_2}}{\partial y}\right)-\left(\dfrac{\partial}{\partial x}\left(D_c\dfrac{\partial C_{O_2}}{\partial x}\right)+\dfrac{\partial}{\partial y}\left(D_c\dfrac{\partial C_{O_2}}{\partial y}\right)\right)=-\left(R_1+3R_2\right)\\ \left(u\dfrac{\partial C_{H_2O}}{\partial x}+v\dfrac{\partial C_{H_2O}}{\partial y}\right)-\left(\dfrac{\partial}{\partial x}\left(D_c\dfrac{\partial C_{H_2O}}{\partial x}\right)+\dfrac{\partial}{\partial y}\left(D_c\dfrac{\partial C_{H_2O}}{\partial y}\right)\right)=6\left(R_1+R_2\right)\end{cases} \tag{6}$$

Furthermore, thermodynamic data for the energy balance equations were calculated based on the polynomial expressions shown in Equation (7) – (9) (Gordon and McBride, 1972).

$$C_{p,i} = R_g \sum_{j=1}^{5} a_j T^{j-1} \tag{7}$$

$$h_i = R_g \left(\sum_{j=1}^{5} \frac{a_j T^j}{j} + a_6 \right) \tag{8}$$

$$S_i = R_g \left(a_1 Ln(T) + \sum_{j=2}^{5} \frac{a_j T^{j-1}}{j-1} + a_7 \right) \tag{9}$$

A set of seven coefficients per species was taken as input for the above polynomials for different temperature intervals (GRI-Mech). In addition to thermodynamic properties, transport properties were used for simulation of the space-dependent reactor model. Transport properties such as binary diffusivities, viscosity, and thermal conductivity were defined as the functions of temperature, pressure, and composition using kinetic gas theory for the reacting gas mixture. In this regard, the diffusivities and gas viscosity are calculated based on Equations (10) and (11), respectively (Dhanushkodi *et al*., 2008).

$$D_c = 2.695 \times 10^{-3} \times \frac{\sqrt{T^3 \left((M_A + M_B)/(2 \times 10^3 \times M_A M_B) \right)}}{p \sigma_A \sigma_B \Omega_D} \tag{10}$$

$$\eta = 2.699 \times 10^{-6} \times \frac{\sqrt{T(1 \times 10^3 M)}}{\sigma^2 \Omega_V} \tag{11}$$

Solution Methodology

In this study, the system of partial differential equations (PDEs) was solved by Comsol Multiphysics software using the finite element method (FEM), where Lagrange-quadratic interpolation elements were used to form the finite element interpolation functions. In order to solve the system of equations, the fully coupled stationary solver with Direct (UMFPACK) module as a linear solution method starts from an initial guess and applies Newton-Raphson iterations until the solution has converged. Hence, the maximum iteration number and relative tolerance of 25 and 1×10^{-6}, respectively, were set as operational solver parameters for the nonlinear setting of automatic linearity module with Damped Newton to solve the possible nonlinear system of equations. Furthermore, Elimination was chosen for Constraint handling method and no type of scaling was considered for automatic solution form, which was adequate to guarantee the steady solution of the proposed model.

Mesh

Free meshes with triangular (advancing front) elements were used to mesh the two-dimensional space in which gas has an upward laminar flow beside the catalyst layer. It should be noted that free meshes are ones that are adaptive in the case of different geometries. Triangular elements with maximum element size of 0.2 mm applied in the catalyst layer are smaller than the bulk elements with maximum element size of 0.5 mm as a result of chemical reaction being done in this narrow catalytic space, which needs to have a more accurate solution. Also, a maximum element size scaling factor of 0.3 was chosen to have a smaller mesh beside the boundaries. In order to avoid possible errors resulting from discontinuity of flow pattern between two subdomains with different mesh sizes, the element growth rate was set to 1.2. As we can see in Figure 3 (B), mesh size increases with distance from the catalyst layer to the subdomain interior. Moreover, the mesh curvature factor, mesh curvature cutoff and resolution of narrow region were taken to be 0.25, 0.0003 and 1, respectively, to have more stable solution.

Grid Independence Analysis

In order to investigate the independency of grids from the solution of problem, the conversion of NO versus different mesh sizes was depicted, which has been shown in Figure 4.

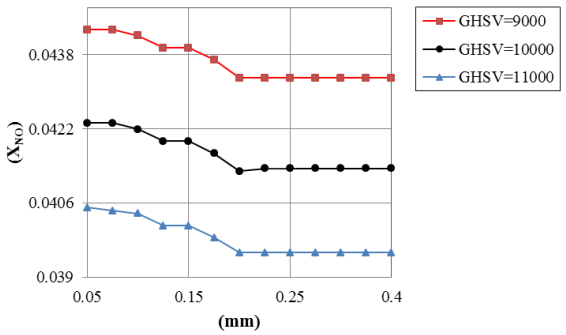

Figure 4: Grid independence analysis.

As shown, mesh size through the catalyst layer varied between 0.05 mm and 0.4 mm. As we can see, by increasing the mesh size, NO conversion fell due to the lack of accuracy with coarser meshes and remained approximately steady for mesh sizes less than 0.2 mm, which in turn indicates the independency of elements for the numerical solution.

Model Validation

In order to evaluate the validation of simulation data, the simulated conversion values of NO in the catalytic filter medium were compared with empirical results obtained from published experiments. The following reaction rate expressions were considered for kinetic calculation of two paralleled reactions (Equations (1) and (2)) in the simulation setup (Schaub *et al.*, 2003):

$$R_1=k_1C_{NO}\frac{aC_{NH_3}}{1+aC_{NH_3}} \tag{12}$$

$$R_2=k_2C_{NH_3} \tag{13}$$

where,

$$k_j=k_{j0}\exp\left(-\frac{E_j}{R_gT}\right) \tag{14}$$

$$a=a_0\exp\left(-\frac{A}{R_gT}\right). \tag{15}$$

The values of the constant parameters used in Equations (14) and (15) are presented in Table 3. As we can see in Figure 5, the simulated values of NO conversion agree well with the experimental data with a maximum average deviation of about 1%.

In order to evaluate the kinetic behavior of reactions, both reaction rates at different temperatures were calculated for equal NO and NH_3 inlet concentration values according to Equations (12) and (13) and are shown in Figure 6. The maximum point in R_1 reflects the fact that, although for temperatures less than 400 ºC, R_1 is more than R_2, at higher temperatures R_2 has higher values. Since our goal is to gain more NO reduction, this figure indicates that having high temperature does not always favor more NO conversion. But, it is not the main reason that lures us into investigation of SCR of NO as the concentrations of reactants vary unequally during these competitive reactions. As we can see in the following sections, the consumption of NH_3 is the primary key factor which influences NO conversion along the gas flow through both catalytic reactors. We also see the effect of various parameters on NO reduction with respect to NH_3 conversion.

Table 3: Parameter values in the rate equations.

E_1=60 kJ/ mol	$k_{20}=6.8\times10^{7}$ s^{-1}
E_2=85 kJ/ mol	A=-243 kJ/ mol
$k_{10}=1\times10^{6}$ s^{-1}	$a_0=2.68\times10^{-17}$ m^3/mol

Source: (Schaub *et al.*, 2003).

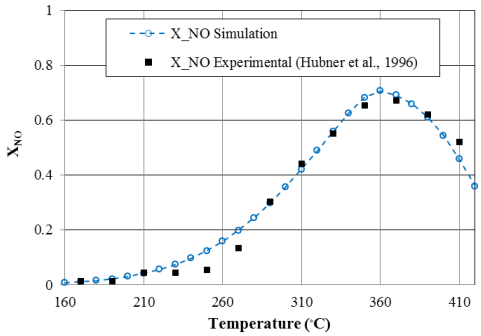

Figure 5: The validation of simulation data with experimental results from catalytic filter candle experiments using ceramic material in a bench-scale test facility ($C_{NO\_in}=C_{NH3\_in}$= 350 ppm, C_{O2_in}=7.6 vol.%, GHSV=11000 h^{-1}, u_{eff}= 0.047 – 0.073 m/s). Reprinted (adapted) with permission from Nahavandi (2014). Copyright (2014) American Chemical Society.

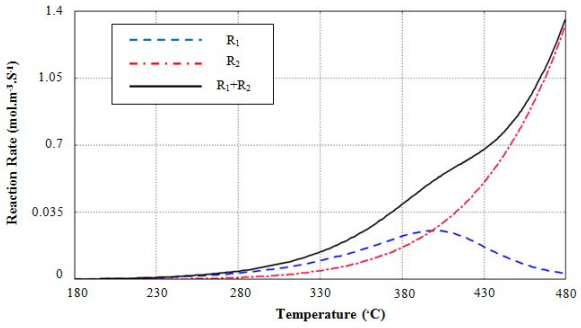

Figure 6: Calculated values of reaction rates R_1 and R_2 for inlet concentration values, conditions: see Figure 5.

SIMULATION RESULTS

The set of steady-state governing equations together with proposed chemical reaction rates were solved simultaneously using Comsol Multiphysics software. Simulation results showed that SCR conversion is substantially under the effect of various

operational conditions. Hence, the influence of operating parameters was investigated individually to identify the extent to which they could be effective on SCR performance.

Effect of Temperature

As indicated, temperature has a strong effect on the rate of two SCR reactions owing to its impact on reaction rate constants obeying the Arrhenius law. The simple expectation is that more NO conversion occurs at higher temperature. However, this is no longer the case even for temperatures less than 400 ºC, as shown by the intersection of two reaction curves in Figure 6. Since two competitive SCR reactions are parallel and ammonia is being consumed simultaneously in both R_1 and R_2, different NO conversions are obtained at different operating temperatures as a result of the decreasing concentration of NH_3 along the reactor. Figure 7 (A), (B) and (C) show the variation of NO and NH_3 concentrations along the reactor at three different temperatures. Figure 7 (D) shows the variation of their concentration along the cross-section shown in Figure 7 (A) for different operating temperatures. As we can see in Figure 7 (D_1) and (D_2), by raising the temperature to 360 ºC, NO and NH_3 concentrations plummet, so that no ammonia is left by the end of the channel.

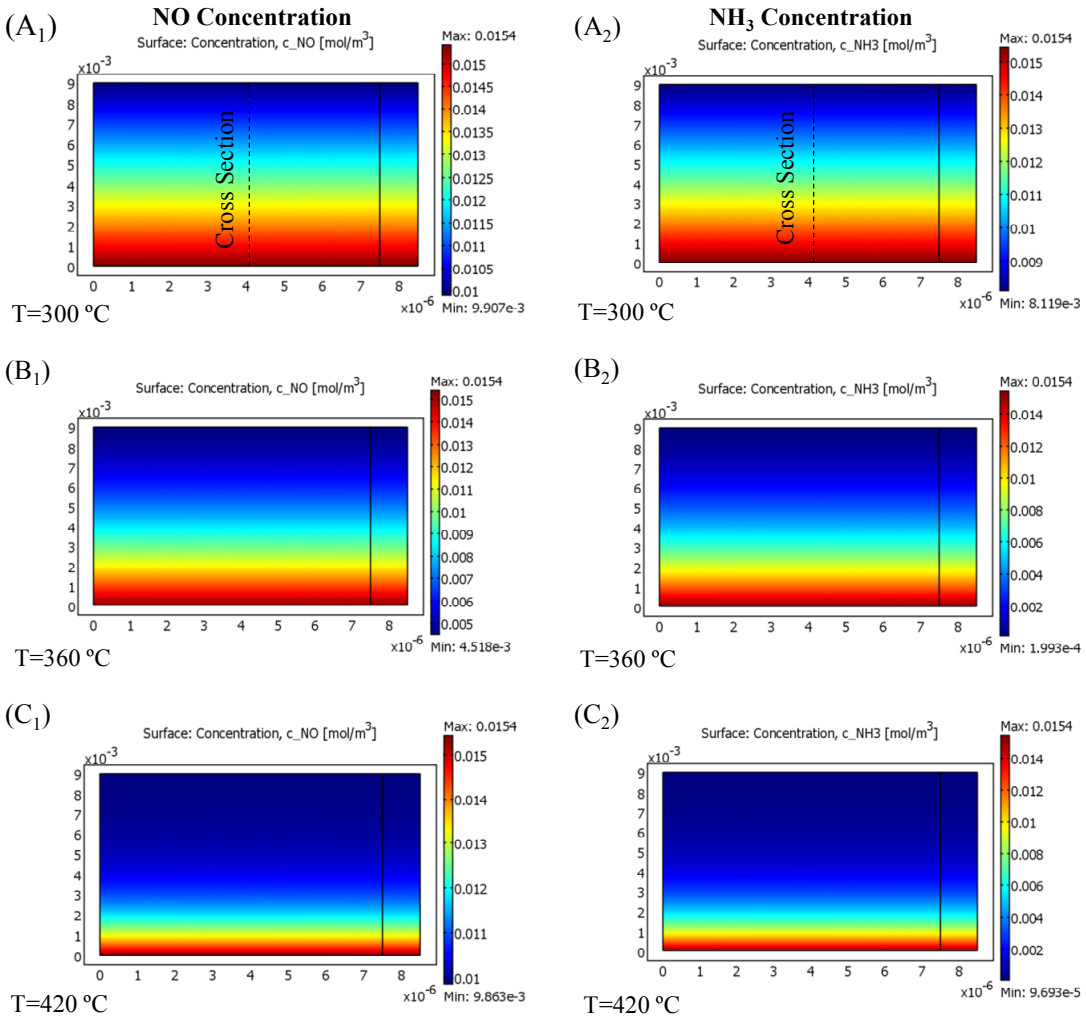

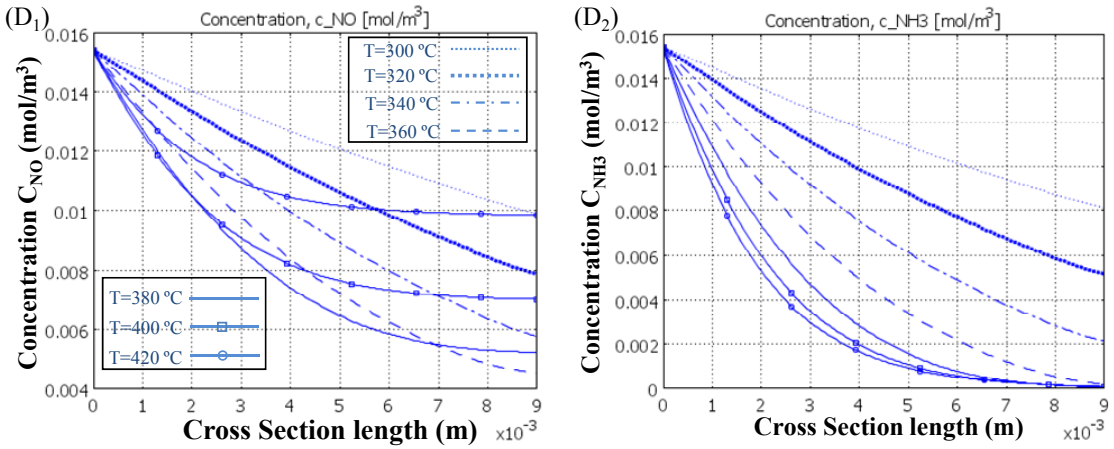

Figure 7: Effect of temperature; Variation of NO and NH_3 concentration through the catalytic filter (A, B, C) and along the cross section (D) for different applied temperatures, conditions: see Figure 5.

Therefore, at 360 ºC, NO has a maximum conversion and its concentration falls to a low of 0.0045 (mol/m^3) or its minimum value. Nevertheless, something different happens for temperatures up to 360 ºC when the rate of the first reaction (R_1) falls, leading to a greater NO outlet concentration at higher temperatures. In contrast, NH_3 is consumed more rapidly according to R_2, but as R_1 slows down, its concentration does not change significantly for temperatures up to 360 ºC. This trend can be seen in Figure 8 (A_1). As shown, by increasing temperature, all trends with different gas velocities rise and, after a maximum, they begin to fall. Focusing on maximum area can reveal more details about what really happens, Figure 8 (B_1). As illustrated, all curves have a descending trend after ammonia is used up completely through the channel, Figure 8 (B_2). Then they all converge into one single curve at 370 ºC, namely the falling point and decrease with a faster descending rate. Actually, there are two areas ahead of the maximum point; the former is due to depletion of NH_3 until reaching 370 ºC and the latter is due to the fall in R_1 that causes all curves to plunge with a single steep trend. The reason why NO conversion declines moderately with the increase of temperature after full consumption of ammonia (Maximum Point of each curve) until reaching the falling point (370 ºC) is the fact that, by using up all ammonia before reaching the end of channel, less catalyst volume is used for catalytic reactions and so less NO is converted. This does not happen when the length of the reactor is adequately long and, as we can see later in the case of the honeycomb reactor, NO conversion is less sensitive to this fact and the curve levels off after the maximum point. As shown in Figure 8 (A_1), after full consumption of NH_3 at the maximum point, the greater the temperature, the lower the conversion. Therefore, one can split up the reactor operating temperature range into three sections in which different conversions of NO occur: NO is reduced along the reactor until all NH_3 is completely consumed (First Section); after that, both reactions stop and the rest of the reactor will remain untouched and so is ineffective. By raising the temperature, less and less of the reactor takes part in SCR of NO, resulting in a moderately lower conversion (Second Section). Then, at higher temperatures, the reaction rate of NO (R_1) decreases and NO conversion plunges steeply (Third Section). These sections can be equivalent to the three parts of each NO conversion curve shown in Figure 8 (B_1) and (B_2). As seen, the second section of each curve is shortened by increasing the gas velocity and it has lower values; therefore, gas velocity has its own effect on NO conversion.

Effect of Gas Velocity

As mentioned, NO conversion varies upon changing the temperature, but there are some parameters which can influence this variation. Gas Hourly Space Velocity (GHSV) is one of these factors since it can change the residence time of reacting components in chemical reactors and so change their conversions. As usual, reducing the residence time by raising the gas velocity, the reactants` conversion should decrease. Hence, the conversion of NO and NH_3 drops off upon increasing the GHSV, which is shown in Figure 8 for a catalytic filter reactor. But even so, conversion variations are not the same for all temperatures with different gas velocities. According to Figure 6, the rate of both reactions at low temperatures tends towards zero and so the gas velocity can

fail to change the reactant conversion owing to a lack of kinetic driving force. On the other hand, at high temperatures the second reaction rate (R_2) increases while the first one (R_1) decreases, which results in the lack of NH_3 and a plummet in NO conversion; so again the GHSV has no major effect on conversion. Therefore, gas velocity in parallel with temperature controls the value of conversion. As we can see in Figure 8 (A_1) and (A_2), the change of GHSV for temperatures less than 190 ºC and molre than 360 ºC makes relatively no difference. In contrast, beside the maximum point, where NO conversion peaked at around 0.7 and NH_3 reached the value of 90% for a GHSV of 3000, gas velocity has the most significant influence on changing the conversions. As shown in Figure 8 (B_1), at a temperature of 330 ºC, upon raising the GHSV from 3000 to 11000, the maximum NO conversion drops by up to 15%. Applying higher temperatures bridges the gap between curves and makes them converge into one single curve. Added to this, another important point is that, upon increasing the gas velocity, the maximum conversion declines and occurs at higher temperature. The reason why it occurs at higher temperature is that an increased gas velocity reduces the possibility of complete NH_3 consumption by the end of the reactor, so the NO conversion diminishes. Although the increase in temperature increases reaction rates that can neutralize to some extent the effect of the increase in gas velocity, as residence time decreases and the major part of the inlet gas goes through the empty space of the reactor faster than through the catalyst porous layer, a lower NO conversion is obtained.

This phenomenon can be seen more obviously in Figure 9 (D_2), which shows the gas velocity field through the honeycomb reactor along the cross section in Figure 9 (A). As shown, gas exits the reactor through empty free space more significantly when it has higher velocities, which is followed by a lower NO conversion that results in higher output concentrations, Figure 9 (D_1). This figure also shows the GHSV influence on the variation of gas flow velocity field and NO concentration as contour plots. As seen, the gas flow through free space is greater under the effect of velocity variation than in the catalyst porous layer. The velocity field has a reverse parabolic trend for flow through the catalyst porous space in comparison with the inner free space of the reactor due to its continuous boundary condition at the interface between the porous medium and free space, which causes the curves to have negative first and second derivatives. In comparison, the catalyst layer has a negative first and a positive second derivative due to the no slip boundary condition on the right hand side of catalyst layer.

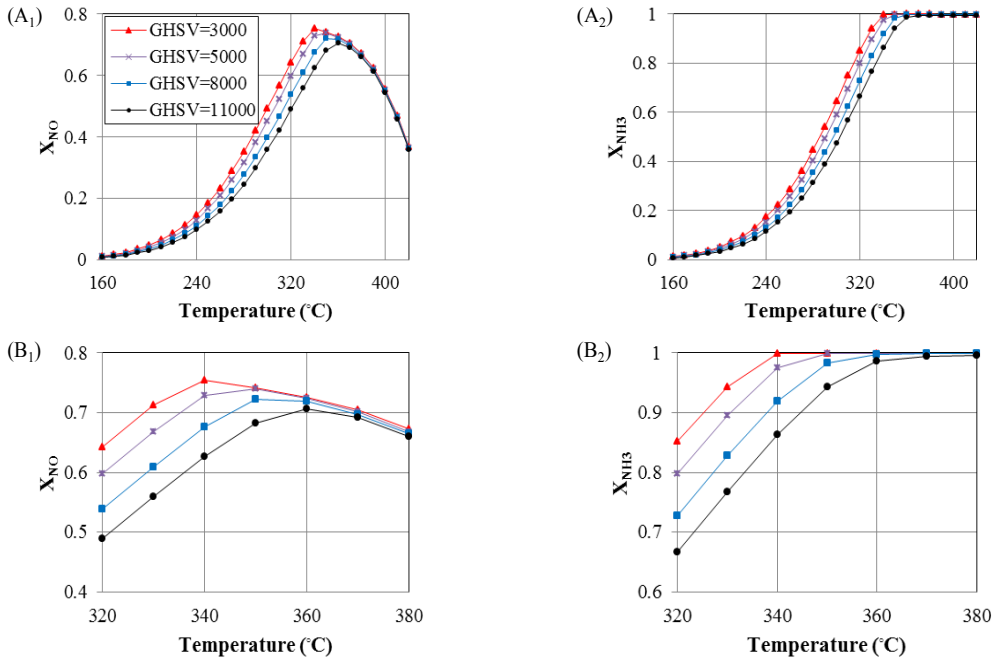

Figure 8: Evaluation of the effect of GHSV on conversion versus the gas temperature in the catalytic filter, $C_{NO\_in}=C_{NH3\_in}=350$ ppm, $C_{O2\_in}=7.6$ vol.%, $\varepsilon_p=0.95$, $k=10^{-8}$ m^2, $d_{chan}=0.015$ mm, $d_{cat}=0.001$ mm, L=9 mm, $P_{in}=1$ atm.

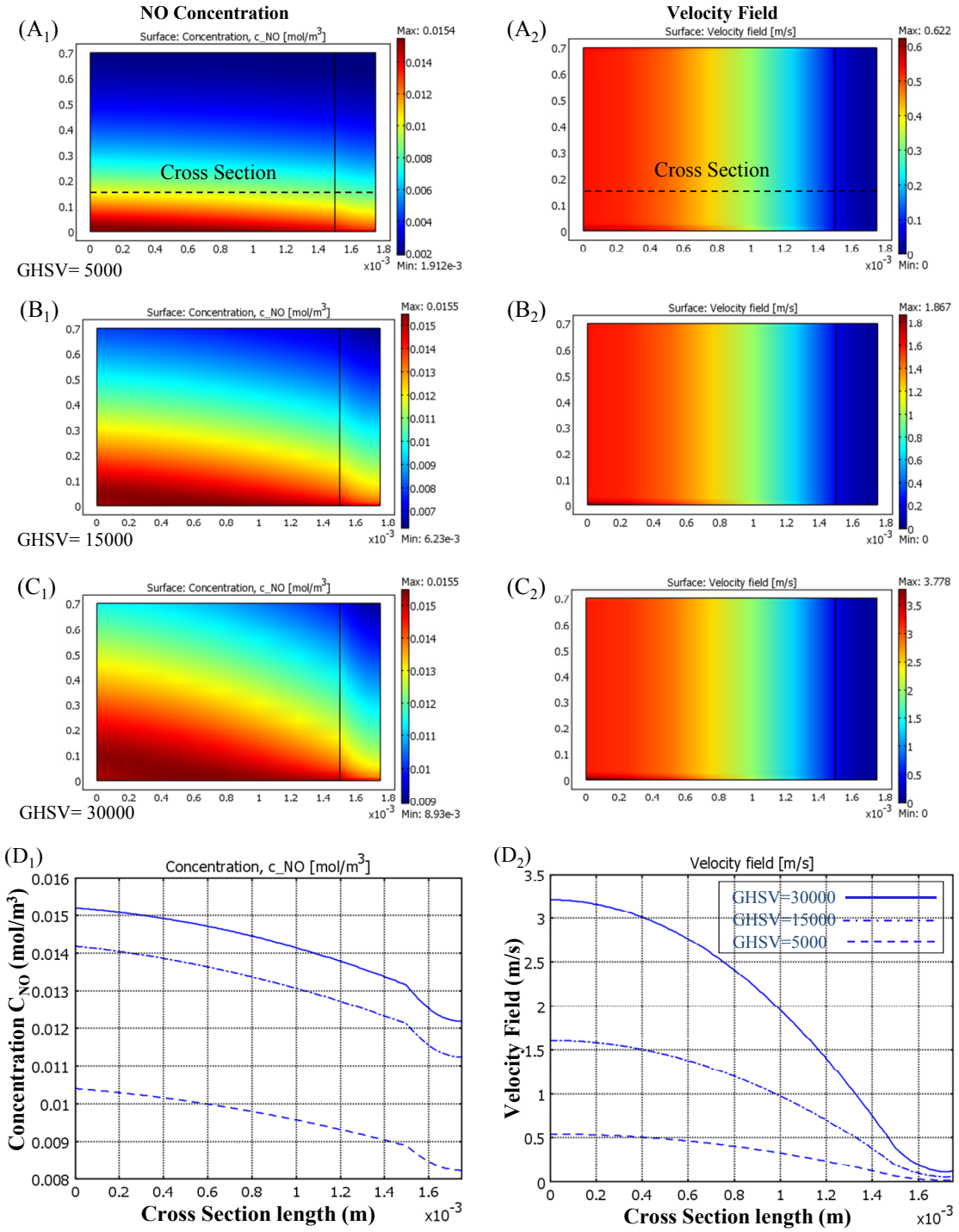

Figure 9: Effect of Gas Velocity; Variation of NO concentration (left column) and velocity field (right column) through the honeycomb reactor (A, B, C) and along the cross section (D) for different applied GHSV, C_{NO_in}=C_{NH3_in}= 350 ppm, C_{O2_in}=7.6 vol.%, ε_p=0.95 , k = 10^{-8} m^2, d_{chan}=3 mm, d_{cat}=0.5 mm, L=0.7 m, T=240 ºC, P_{in}= 1 atm.

The honeycomb reactor also undergoes changes similar to the catalytic filter regarding gas velocities. Once again, upon full consumption of ammonia, NO conversion with different GHSVs starts to decrease and, at higher temperatures, they converge into one descending curve. But, in this case, there is a special difference in the descending trend of NO conversion. As we can see in Figure 10 (A), NO conversions for temperatures from 240 ºC and 280 ºC to 340 ºC, respectively for low GHSVs of 5000 and 15000 are relatively level. As mentioned earlier, the reason for the moderate falling trend after maximum point is that, at higher temperatures, NH_3 is used up closer to the inlet of the reactor, so the chemical reactions occurs in less catalyst space and therefore conversion decreases. Here, because the length of the honeycomb reactor is much longer than its width, around two orders of magnitude, at low GHSVs the NO conversion levels off with less effect from catalyst usage space and a lengthening of the second section of the curve after the maximum point. Afterward, all curves converge into one steep falling trend due to the decline of R_1. This fact can also be seen in the next section where the concentration influences on the conversion is considered.

Effect of Inlet Concentration

The concentration of gas toxic pollutants is one of the most crucial factors in selection of the best operational condition for contaminant elimination. So, in this section, we examine the SCR of NO under the effect of different NH_3 and NO concentrations at various operating temperatures in the catalytic filter and honeycomb reactor. As mentioned earlier, there are three sections of NO conversion regarding gas temperature. Here, as seen in Figure 11, with a decrease of NH_3 concentration, NO conversion generally diminishes, so that the maximum conversion plunges and shifts towards lower temperatures; this causes the second section to lengthen and level off at a relatively similar value. Moreover, despite the changes in ammonia concentration, the falling point does not change and still occurs at 340 ºC because, as mentioned earlier, it consists of R_1 which relies on the operating temperature according to the Arrhenius Law for the reaction rate constant. Upon raising the ammonia inlet concentration, NO conversion increases, more significantly for temperatures between 180 and 340 ºC, Meanwhile the maximum point matches the falling point and the maximum operating conversion is reached. In contrast, at higher temperatures, R_1 begins to decrease and conversion is less and less affected by raising the NH_3 concentration.

In order to evaluate the effect of concentration on conversion more precisely, the variation of NH_3 and NO concentrations along the cross section through the honeycomb reactor has been calculated with the low NH_3 inlet concentration of 200 ppm as shown in Figure 12. This figure reveals more facts about the fluctuating trends of reactant conversion versus changing temperature. As shown, the NO outlet concentration decreases upon increasing the temperature up to 260 ºC. By raising the temperature to 300 ºC and 340 ºC, NO and NH_3 final concentrations do not change to a similar output value, although this happens at a shorter distance of 0.4 m for these temperatures than that of 0.6 m for 260 ºC. On the other hand, for temperatures of 380 ºC and 420 ºC, the NO output concentration increases due to a smaller R_1. Even so, their falling trends level off once again at 0.4 m from the inlet of the reactor. As indicated earlier, raising the temperature decreases the ammonia slip, while NO concentration may either increase or decrease with temperature. This issue can be clearly seen in Figure (12). Thus, as the operating temperature rises, the concentration of outlet ammonia decreases significantly.

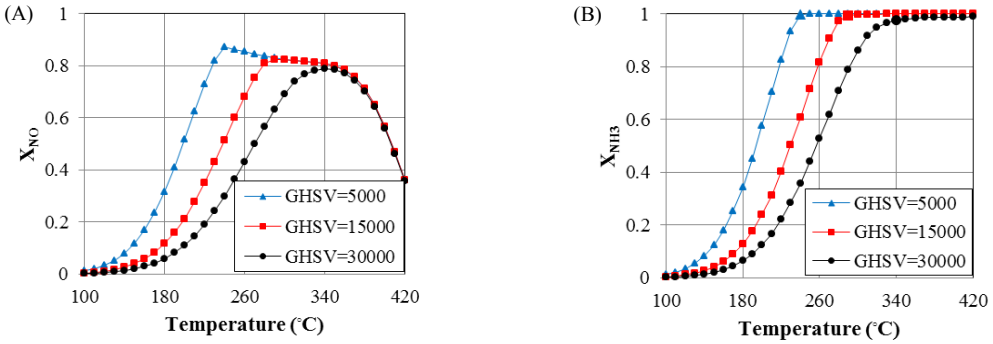

Figure 10: Evaluation of the effect of GHSV on conversion versus gas temperature in the honeycomb reactor, conditions: see Figure 9.

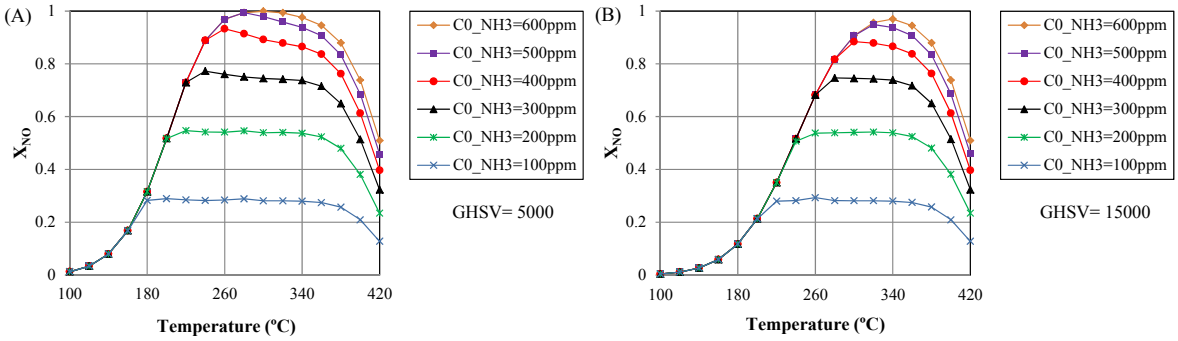

Figure 11: Effect of NH_3 inlet concentration on NO conversion in the honeycomb reactor, C_{NO_in}= 350 ppm, other conditions: see Figure 9.

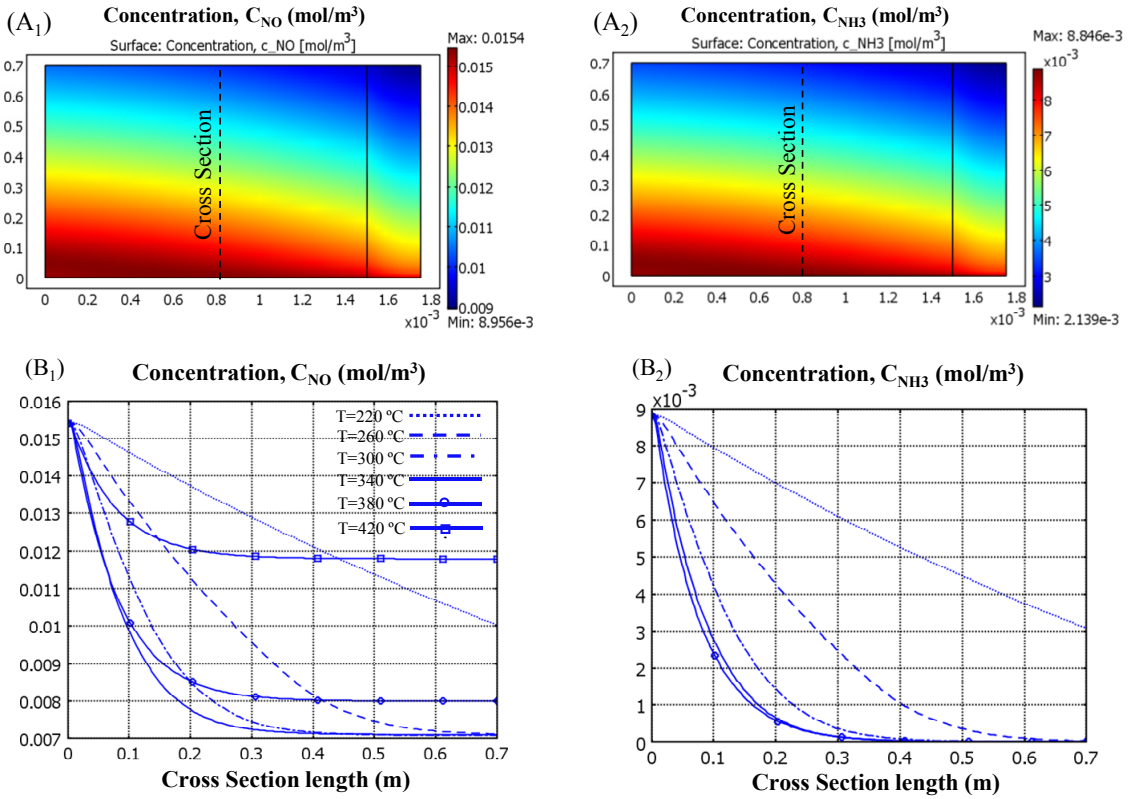

Figure 12: Variation of NO and NH_3 concentrations along the honeycomb reactor, C_{NO_in}= 350 ppm, $C_{NH3\ in}$= 200 ppm, GHSV=15000, other conditions: see Figure 9.

There is also a similar trend in the catalytic filter reactor, but with relatively small differences owing to the short length of this kind of reactor, which results in no level trend in the second section after the maximum conversion. As shown in Figure 13, all conversions, particularly with low ammonia concentrations, present descending trends after the maximum point and start to plummet more steeply at the falling point of 370 ºC. This figure also shows how we can obtain similar conversions with lower temperature and NH_3 inlet concentration to obtain an optimum SCR for NO. For example, an 80% conversion can be achieved at 350 ºC with 400 ppm NH_3 rather than using 700 ppm of ammonia at around 398 ºC.

More NO conversion is not always achieved by raising the NH_3 concentration because the reaction rate (R_1) controls its increase, especially at temperatures less than the maximum point where the reaction has its maximum rate for available ammonia. As shown in Figure 13, for temperatures less than 300 ºC, NO conversion does not change and has a

similar value for all ammonia inlet concentrations. At higher temperatures, as the reaction rate increases, more conversion is gained by adding NH_3 inlet concentration. After the falling point, since R_1 begins to decrease at higher temperatures, less NO conversion can be obtained by raising ammonia. As we can see in Figure 13, for an NH_3 inlet concentration of 700 ppm at 370 ºC the maximum conversion of 0.88 is gained upon raising its concentration even further, the maximum conversion does not increase remarkably, so that it matches the maximum point of NH_3 inlet concentration of 600 ppm. So, upon raising the ammonia concentration, the maximum point for each curve tends to reach the falling point until they cover each other. At this point, the maximum conversion for the reactor under specified conditions is obtained.

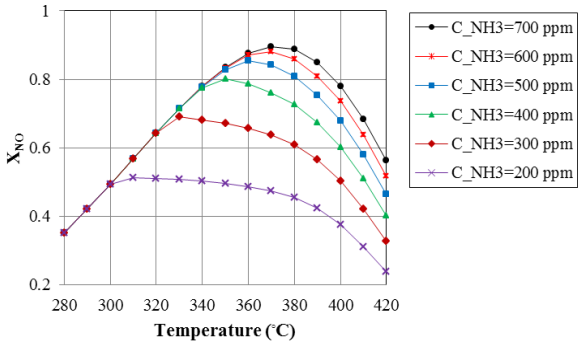

Figure 13: Effect of NH_3 inlet concentration on NO conversion in the catalytic filter, C_{NO_in}= 350 ppm, GHSV=3000, other conditions; see Figure 8.

As mentioned earlier, the SCR process requires accurate control of the ammonia injection rate in the form of the NH_3/NO ratio, so that the application of ratios greater than 1 considerably increases the ammonia slip. In order to show the most appropriate operating conditions, the variation of NO conversion versus the NH_3/NO ratio in the catalytic filter at different operating temperatures is shown in Figure 14 (A). As we can see, by raising the NH_3/NO ratio at temperatures higher than 380 ºC, NO conversion increases, while it levels off at lower temperatures especially at NH_3/NO ratios higher than 1.14, which implies more of the increase in ammonia slip. Moreover, the variation of NO conversion versus the NO/NH_3 ratio is shown in Figure 14 (B). As seen, by increasing the NO/NH_3 ratio, NO conversion decreases more sharply at lower temperatures. Therefore, the increase of NO concentration rather than ammonia, particularly at low operating temperatures, considerably diminishes the SCR efficiency. Figure 15 (A) and (B) also present similar trends for the honeycomb reactor.

Effect of Channel and Catalyst Layer Width

As mentioned earlier, a large amount of the input gas in the reactor passes through vacant space with higher bulk velocity than the little amount that passes through the porous medium of the catalyst layer, Figure 10 (D). So, the widths of the channel and catalyst layers play a crucial role in the level at which a catalytic reactor can be effective in reduction of reacting components. Conceivably, the effect of channel width strongly depends on gas velocity through the reactor, which is known as GHSV. As shown in Figure 16, at low gas velocities the width does not make a considerable difference in NO conversion and so at a GHSV about 2500 all curves converge with each other. Conversely, at higher GHSVs, the channel and catalyst layer widths are more decisive.

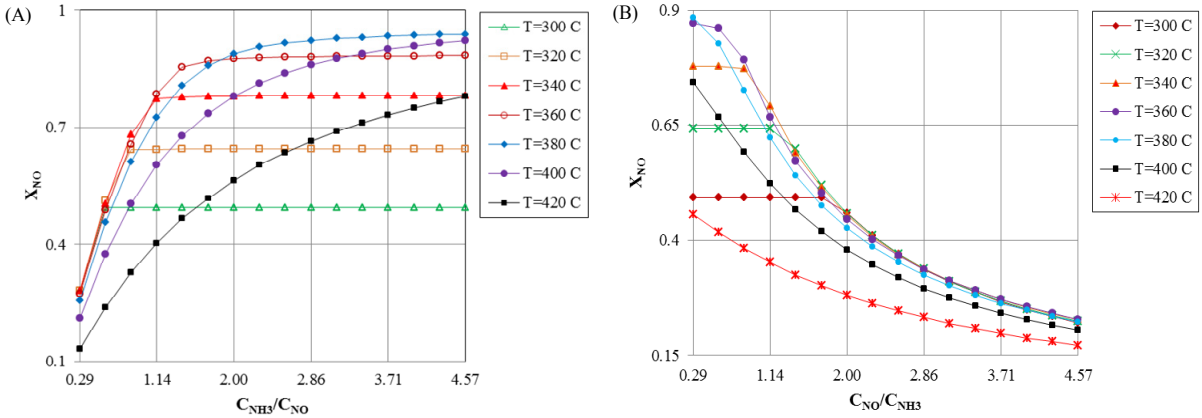

Figure 14: Effect of NO and NH_3 inlet concentrations on NO conversion at different temperatures in the catalytic filter, GHSV=3000, (A) C_{NO}=350 ppm, (B) C_{NH3}=350 ppm, other conditions: see Figure 8.

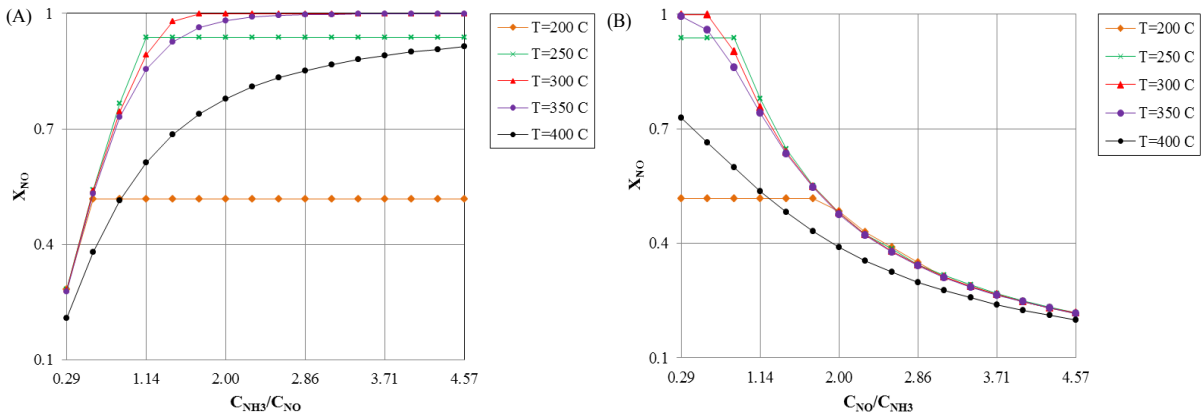

Figure 15: Effect of NO and NH_3 inlet concentrations on NO conversion at different temperatures in the honeycomb reactor, GHSV=5000, (A) C_{NO}=350 ppm, (B) C_{NH3}=350 ppm, other conditions: see Figure 9.

Overall, the trends with different channel and catalyst layer widths are a decrease upon raising the GHSV. Nevertheless, the NH_3-SCR of NO in channels with narrower widths and wider catalyst layers is less affected by an increase in gas velocity, although the effect of channel width outweighs the influence of catalyst layer thickness. As we can see in Figure 16, by increasing GHSV, NO conversion plunges more rapidly in the channel width of 12 mm than at narrow channel widths of 3, 6 and 9 mm, although in each case NO conversion for the thicker catalyst layer has higher values.

Effect of Reactor Length

Reactant conversion through a catalytic reactor is, to a large extent, under the effect of gas velocity. Hence the residence time of reactants can be changed by applying different lengths of reactor and the length of the reactor channel leads to different conversions for a specific GHSV. This is more obvious at higher GHSVs and lower residence times, where full conversion of reactant is not obtained and is more sensitive to the length of channel. In contrast, by increasing the residence time due to a decrease of gas velocity, the effect of channel length on conversion diminishes, as shown in Figure 17. A low GHSV around 2000, all curves for different lengths of reactor channels converge into a one horizontal line owing to the full conversion of NO before reaching the end of the reactor. By increasing the GHSV, all conversion curves start to decrease, but at different points due to the different channel lengths.

Where NO reacts thoroughly is at 0.7, 1.4 and 3 m of the reactor channel, respectively, for GHSVs of 2000, 6000 and 12000. However, the residence time is not the only effect caused by channel length since the curves descend with different slopes. As indicated earlier in Figure 10, a large proportion of the input reacting gas exits from the reactor with a low possibility of catalyst engagement due to a higher flow rate in the free space than in the catalyst layer. This can be intensified more significantly at short channel lengths and, as shown in Figure 17, NO conversion begins to fall steeply at low GHSV of 2000 for a channel length of 0.7 m. This happens with much lower descending slopes for channel lengths of 1.4 and 3 m at GHSVs of 6000 and 12000, respectively. As shown, the honeycomb reactor with channel length of 3 m has the minimum effect of free space, so it presents a linear falling trend with an increase in GHSV. Its gas flow is known as a uniform plug flow, generally.

Effectiveness of Operating Variables

Although each of the operating parameters has its own effect on SCR performance, it is important to identify variables that can most effectively influence the NO conversion, which is the primary aim of this study. In this regard, the maximum variations of NO conversion due to the variation of different operating variables are presented in Table 4. As seen, NO conversion increases 0.85 and 0.74 as the temperature rises from 100 ºC to 240 ºC and from 160 ºC to 340 ºC, respectively, in the honeycomb reactor and catalytic filter medium. NO conversion can also be substantially altered by more than 0.7, through an NH_3/NO ratio variation from 0.29 to 4.57 in both catalytic reactors. Therefore, the SCR process is most significantly affected by operating temperature and NH_3/NO ratio.

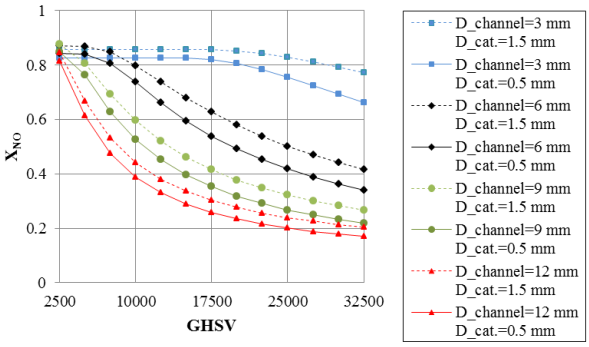

Figure 16: Effect of channel and catalyst layer width on NO conversion in the honeycomb reactor, T=300 ºC, d_{chan}=3 mm, d_{cat}=0.5 mm, other conditions: see Figure 9.

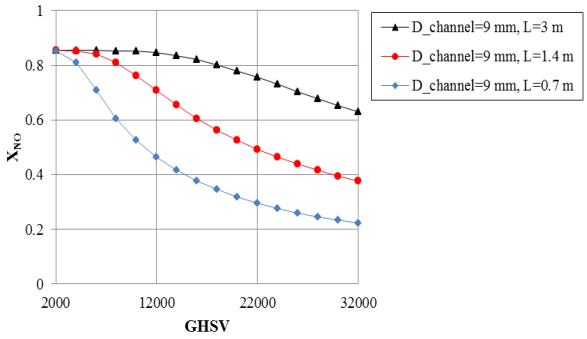

Figure 17: Effect of reactor channel length on NO conversion in the honeycomb reactor, T=300 ºC, d_{chan}=9 mm, d_{cat}=0.5 mm, other conditions: see Figure 9.

Table 4: The maximum variation of NO conversion for different operating parameters.

Variables	Catalytic Filter		Honeycomb Reactor	
	Operating range	$\Delta X_{max.}$	Operating range	$\Delta X_{max.}$
T	160 ºC to 340 ºC (C_{NO}=C_{NH3}=350 ppm)	0.7425	100 ºC to 240 ºC (C_{NO}=C_{NH3}=350 ppm)	0.8585
GHSV	3000 to 11000 (C_{NO}=C_{NH3}=350 ppm)	− 0.1535	5000 to 30000 (C_{NO}=C_{NH3}=350 ppm)	− 0.5767
C_{NH3}/ C_{NO}	0.29 to 4.57 (C_{NO}=350 ppm)	0.7109	0.29 to 4.57 (C_{NO}=350 ppm)	0.7215
$D_{channel}$	-	-	3 to 12 mm ($D_{cat.}$=1.5)	− 0.59
$D_{cat.}$	-	-	0.5 to 1.5 mm ($D_{channel}$=3 mm)	0.10
L	0.009 to 0.02 m ($D_{cat.}$=0.001, $D_{channel}$=0.015 mm)	0.1257	0.7 to 3 m ($D_{cat.}$=0.5, $D_{channel}$=9 mm)	0.461

CONCLUSIONS

SCR performance depends on the temperature and reactant concentration of the flue gas mixture that flows into the SCR reactor. NO conversion increases upon raising the NH_3/NO ratio at relatively high operating temperatures, while it remains constant at low temperatures with a high level of ammonia slip emitted from the reactor discharge. Although the ammonia slip can be reduced by increasing the temperature, the NO conversion in a SCR catalyst may either increase or decrease, depending on the particular temperature range and the type of catalyst. Based on the simulation results, optimum SCR performance for NO reduction with minimum ammonia slip in both the catalytic filter medium and the honeycomb reactor could be achieved by applying an NH_3/NO molar ratio of about 1.14 in certain operational conditions, which conforms to the experimental data obtained for this ratio in NH_3-SCR catalysts.

NOMENCLATURE

A	Frequency factor
C_i	Concentration (mol/m^3)
C_p	Heat capacity at constant pressure (J/(kg.K))
C_{p_i}	Species' heat capacity (J/(mol.K)
D_c	Diffusion coefficient (m^2/s)
E_j	Activation energy (J/mol)
g	gravitational acceleration (m/s^2)
h_i	Species' molar enthalpy (J/mol)
I	Unit vector
k	Thermal conductivity (W/m.K)
k_i	Reaction rate constant
k_p	Permeability (m^2)
L	Catalyst length (m)
M_A	Molar weight of A (kg/mol)
M_B	Molar weight of B (kg/mol)

n	Normal unit vector
p	Pressure (Pa)
R	Reaction rate (mol/(m^3.s))
R_g	Universal gas constant: 8.31441 (J/(mol. K))
s_i	Species' molar entropy (J/(mol.K)
T	Temperature (K)
U	Velocity (m/s)
X	Conversion

Greek Letters

ε_p	Porosity
η	Dynamic viscosity (Pa.s)
ρ	Fluid density (kg/m^3)
σ	Characteristic length of the Lennard-Jones interaction potential: 10^{-10} (m)
σ_A	Molecular diameter of A (m)
σ_B	Molecular diameter of B (m)
Ω_D	Collision integral
Ω_V	Collision integral

Abbreviations

SCR	Selective Catalytic Reduction
$DeNO_x$	NO_x removal
GHSV	Gas Hourly Space Velocity
UMFPACK	Unsymmetric MultiFrontal method

REFERENCES

Baukal Jr, C. E., Ed. The John Zink Hamworthy Combustion Handbook: Applications, CRC Press, Boca Raton, FL (2013).

Ciardelli, C., Nova, I., Tronconi, E., Chatterjee, D., Bandl-Konrad, B., Weibel, M., Krutzsch, B., Reactivity of NO/NO_2 -NH_3 SCR system for diesel exhaust aftertreatment: identification of the reaction network as a function of temperature and NO_2 feed content. Applied Catalysis B: Environmental, 80-90 (2007).

Dhanushkodi, S. R., Mahinpey, N. and Wilson, M., Kinetic and 2D reactor modeling for simulation of the catalytic reduction of NO_x in the monolith honeycomb reactor. Process Saf. Environ. Prot., 303-309 (2008).

Gieshoff, J., Schäfer-Sindlinger, A., Spurk, P. C., Van Den Tillaart, J. A. A., and Garr, G., Improved SCR systems for heavy-duty applications. SAE Transactions, 109, 73-80 (2000).

Gordon, S. and McBride, B. J., Computer program for calculation of complex chemical equilibrium compositions. NASA (1972).

GRI-Mech 3.0: http://www.me.berkeley.edu/gri-mech/.

Hubner, K., Pape, A. and Weber, E. A., Simultaneous removal of gaseous and particulate components from gases by catalytically activated ceramic filters. Conf. Proc. High Temp. Gas Cleaning, 267-277 (1996).

Kobayashi, Y., Tajima, N., Nakano, H. and Hirao, K., Selective catalytic reduction of nitric oxide by ammonia: The activation mechanism. The Journal of Physical Chemistry, B, 108, 12264-12266 (2004).

Lietti, L., Nova, I., Camurri, S., Tronconi, E. and Forzatti, P., Dynamics of the SCR-$DeNO_x$ reaction by the transient-response method. AIChE Journal, 43, 2559-2570 (1997).

Nahavandi, M., Selective catalytic reduction of nitric oxide by ammonia over V_2O_5/TiO_2 in a hollow cylindrical catalyst under enhancing effect of electrohydrodynamics: A kinetic modeling study. Industrial & Engineering Chemistry Research, 53, 12673-12688 (2014).

Nam, J. G., Static characteristics of a urea-SCR system for NO_x reduction in diesel engines. International Journal of Automotive Technology, 8, 283-288 (2007).

Neuffer, B. and Laney, M., Alternative Control Techniques Document Update: NO_x Emissions from New Cement Kilns. US Environmental Protection Agency, Office of Air Quality Planning and Standards, Sector Policies and Programs Division (2007).

Nova, I., Beretta, A., Groppi, G., Lietti, L., Tronconi, E. and Forzatti, P., Monolithic Catalysts for NO_x Removal from Stationary Sources. Structured Catalyst and Reactors. Marcel Dekker, New York, 171-214 (2006).

Nova, I., Ciardelli, C., Tronconi, E., Chatterjee, D. and Bandl-Konrad, B., NH_3-SCR of NO over a V-based catalyst: Low-T redox kinetics with NH_3 inhibition. AIChE Journal, 52, 3222-3233 (2006).

Nova, I., Ciardelli, C., Tronconi, E., Chatterjee, D. and Weibel, M., Unifying redox kinetics for standard and fast NH_3-SCR over a V_2O_5-WO_3/TiO_2 catalyst. AIChE Journal, 55, 1514-1529 (2009).

Roduit, B., Baiker, A., Bettoni, F., Baldyga, J. and Wokaun, A., 3-D modeling of SCR of NO_x by NH_3 on vanadia honeycomb catalysts. AIChE Journal, 44, 2731-2744 (1998).

Schaub, G., Unruh, D., Wang, J. and Turek, T., Kinetic analysis of selective catalytic NO_x reduction (SCR) in a catalytic filter. Chemical Engineering

and Processing: Process Intensification, 42, 365-371 (2003).

Seong, H. J., Selective Catalytic Reduction (SCR) of NO by NH_3 in a Fixed-bed Reactor; M. S. Dissertation. The Pennsylvania State University, Pennsylvania (2012).

Tsinoglou, D. and Koltsakis, G., Modelling of the selective catalytic NO_x reduction in diesel exhaust including ammonia storage. Proceedings of the Institution of Mechanical Engineers, Part D: Journal of Automobile Engineering, 221, 117-133 (2007).

Vega, E. M., García, S. O., Sanz, F. V. D., Ammonia selective catalytic reduction of NO in a monolithic reverse flow reactor. Chemical Engineering, 24 (2011).

Winkler, C., Flörchinger, P., Patil, M. D., Gieshoff, J., Spurk, P. and Pfeifer, M., Modeling of SCR denox catalyst: Looking at the impact of substrate attributes. SAE Transactions, 112, 691-699 (2003).

Yun, B. K. and Kim, M. Y., Modeling the selective catalytic reduction of NO_x by ammonia over a vanadia-based catalyst from heavy duty diesel exhaust gases. Applied Thermal Engineering, 50, 152-158 (2013).

Zürcher, S., Hackel, M. and Schaub, G., Kinetics of selective catalytic NO_x reduction in a novel gas-particle filter reactor (catalytic filter element and sponge insert). Industrial & Engineering Chemistry Research, 47, 1435-1442 (2008).